## Research Article

# Frequency-Domain Equalization in Single-Carrier Transmission: Filter Bank Approach

**Yuan Yang,[1] Tero Ihalainen,[1] Mika Rinne,[2] and Markku Renfors[1]**

[1] Institute of Communications Engineering, Tampere University of Technology, P.O. Box 553, 33101 Tampere, Finland
[2] Nokia Research Center, P. O. Box 407, Helsinki 00045, Finland

This paper investigates the use of complex-modulated oversampled filter banks (FBs) for frequency-domain equalization (FDE) in single-carrier systems. The key aspect is mildly frequency-selective subband processing instead of a simple complex gain factor per subband. Two alternative low-complexity linear equalizer structures with MSE criterion are considered for subband-wise equalization: a complex FIR filter structure and a cascade of a linear-phase FIR filter and an allpass filter. The simulation results indicate that in a broadband wireless channel the performance of the studied FB-FDE structures, with modest number of subbands, reaches or exceeds the performance of the widely used FFT-FDE system with cyclic prefix. Furthermore, FB-FDE can perform a significant part of the baseband channel selection filtering. It is thus observed that fractionally spaced processing provides significant performance benefit, with a similar complexity to the symbol-rate system, when the baseband filtering is included. In addition, FB-FDE effectively suppresses narrowband interference present in the signal band.

## 1. INTRODUCTION

Future wireless communications must provide ever increasing data transmission rates to satisfy the growing demands of wireless networking. As symbol-rates increase, the intersymbol interference, caused by the bandlimited time-dispersive channel, distorts the transmitted signal even more. The difficulty of channel equalization in single-carrier broadband systems is thus regarded as a major challenge to high-rate transmission over mobile radio channels. Single-carrier time-domain equalization has become impractical because of the high computational complexity of needed transversal filters with a high number of taps to cover the maximum delay spread of the channel [1]. This has lead to extensive research on spread spectrum techniques and multicarrier modulation. On the other hand, single-carrier transmission has the benefit, especially for uplink, of a very simple transmitter architecture, which avoids, to a large extent, the peak-to-average power ratio problems of multicarrier and CDMA techniques. In recent years, the idea of single-carrier transmission in broadband wireless communications has been revived through the application of frequency-domain equalizers, which have clearly lower implementation complexity than time-domain equalizers [1–3]. Both linear and decision

feedback structures have been considered. In [2, 4–6], it has been demonstrated that the single-carrier frequency-domain equalization may have a performance advantage and that it is less sensitive to nonlinear distortion and carrier synchronization inaccuracies compared to multicarrier modulation.

The most common approach for FDE is based on FFT/IFFT transforms between the time and frequency domains. Usually, a cyclic prefix (CP) is employed for the transmission blocks. Such a system can be derived, for example, from OFDM by moving the IFFT from the transmitter to the receiver [4]. FFT-FDEs with CP are characterized by a flat-fading model of the subband responses, which means that one complex coefficient per subband is sufficient for ideal linear equalization. This approach has overhead in data transmission due to the guard interval between symbol blocks. Another approach is to use overlapped processing of FFT blocks [7–9] which allows equalization without CP. This results in a highly flexible FDE concept that can basically be used for any single-carrier system, including also CDMA [8].

This paper develops high performance single-carrier FDE techniques without CP by the use of highly frequency-selective filter banks in the analysis-synthesis configuration, instead of the FFT and IFFT transforms. We examine the use of subband equalization for mildly frequency-selective

subbands, which helps to reduce the number of subbands required to achieve close-to-ideal performance. This is facilitated by utilizing a proper complex, partially oversampled filter bank structure [10–13].

One central choice in the FDE design is between symbol-spaced equalizers (SSE) and fractionally spaced equalizers (FSE) [3, 14]. An ideal receiver includes a matched filter with the channel matched part, in addition to the root raised cosine (RRC) filter, before the symbol-rate sampling. SSE ignores the channel matched part, leading to performance degradation, whereas FSEs are, in principle, able to achieve ideal linear equalizer performance. However, symbol-rate sampling is often used due to its simplicity. In frequency-domain equalization, FSE can be done by doubling the number of subbands and the sampling rate at the filter bank input [1, 3, 6]. This paper examines also the performance and complexity tradeoffs of the SSE and FSE structures.

The main contribution of this paper is an efficient combination of analysis-synthesis filter bank system and low-complexity subband-wise equalizers, applied to frequency-domain equalization. The filter bank has a complex I/Q input and output signals suitable for processing baseband communication signals as such, so no additional single sideband filtering is needed in the receiver (real analysis-synthesis systems cannot be easily adapted to this application). The filter bank also has oversampled subband signals to facilitate subband-wise equalization. We consider two low-complexity equalizer structures operating subband-wise: (i) a 3-tap complex-valued FIR filter (CFIR-FBEQ), and (ii) the cascade of a low-order allpass filter as the phase equalizer and a linear-phase FIR filter as the amplitude equalizer (AP-FBEQ). In the latter structure, the amplitude and phase equalizer stages can be adjusted independently of each other, which turns out to have several benefits. Simple channel estimation based approaches for calculation of the equalizer coefficients both in SSE and FSE configurations and for both equalizer structures are developed. Further, the benefits of FB-FSEs in contributing significantly to the receiver selectivity will be addressed.

In a companion paper [15], a similar subband equalizer structure is utilized in filter bank based multicarrier (FBMC) modulation, and its performance is compared to a reference OFDM modulation in a doubly dispersive broadband wireless communication channel. In this paper, we continue with the comparisons of OFDM, FBMC, single-carrier FFT-FDE, and FB-FDE systems. The key idea of our equalizer concept has been presented in the earlier work [16] together with two of the simplest cases of the subband equalizer.

The content of this paper is organized as follows: Section 2 gives an overview of FFT-SSE and FFT-FSE. In addition, the mean-squared error (MSE) criterion based subband equalizer coefficients are derived. Section 3 addresses the exponentially modulated oversampled filter banks and the subband equalization structures, CFIR-FBEQ and AP-FBEQ. The particular low-complexity cases of these structures are presented, together with the formulas for calculating the equalizer coefficients from the channel estimates. Also, the channel estimation principle is briefly described.

Section 4 gives numerical results, including simulation results to illustrate the effects of filter bank and equalizer parameters on the system performance. Then detailed comparisons of the studied FB-SSE and FB-FSE structures with the reference systems are given.

## 2. FFT BASED FREQUENCY-DOMAIN EQUALIZATION IN A SINGLE-CARRIER TRANSMISSION

Throughout this paper, we consider single-carrier block transmission over a linear bandlimited channel with additive white Gaussian noise. We assume that the channel has time-invariant impulse response during each block transmission. For each block, a CP is inserted in front of the block, as shown in Figure 1. In this case, the received signal is obtained as a cyclic convolution of the transmitted signal and channel impulse response. Therefore, the channel frequency response is accurately modeled by a complex coefficient for each frequency bin [17]. The length of the CP extension is $P \geq L$, where $L$ is the maximum length of the channel impulse response. The CP includes a copy of information symbols from the tail of the block. This results in bandwidth efficiency reduction by the factor $M/(M+P)$, where $M$ is the length of the information symbol block. In general, for time-varying wireless environment, $M$ is chosen in such a way that the channel impulse response can be considered to be static during each block transmission.

The block diagram of a communication link with FFT-SSE and FFT-FSE is shown in Figure 1. The operations of the equalization include the forward transform from time to frequency domain, channel inversion, and the reverse transform from frequency to time domain. The CP is inserted after the symbol mapping in the transmitter and discarded before equalization in the receiver. At the transmitter side, a block of $M$ symbols $x(m)$, $m = 0, 1, \ldots, M - 1$, is oversampled and transmitted with the average power $\sigma_x^2$. The received oversampled signal $r(n)$ can be written as

$$r(n) = x(n) \otimes c(n) + v(n),$$
$$c(n) = g_T(n) \otimes h_{\mathrm{ch}}(n) \otimes g_R(n). \tag{1}$$

Here $v(n)$ is additive white Gaussian noise with variance $\sigma_n^2$. The symbol $\otimes$ represents convolution, $h_{\mathrm{ch}}(n)$ is the channel impulse response, and $g_T(n)$ and $g_R(n)$ are the transmit and receive filters, respectively. They are both RRC filters with the roll-off factor $\alpha \leq 1$ and the total signal bandwidth $B = (1 + \alpha)/T$, with $T$ denoting the symbol duration.

Generally in the paper, the lowercase letters will be used for time-domain notations and the uppercase letters for frequency-domain notations. The letter $n$ is used for time-domain $2\times$ symbol-rate data sequences and $m$ for symbol-rate sequences, while the script $k$ represents the index of frequency-domain subband signals. For example, in Figure 1, $R_k$ is the received signal of $k$th subband, and $W_k$ and $\widehat{W}_k$ represent the $k$th subband equalizer coefficients of SSE and FSE, respectively.
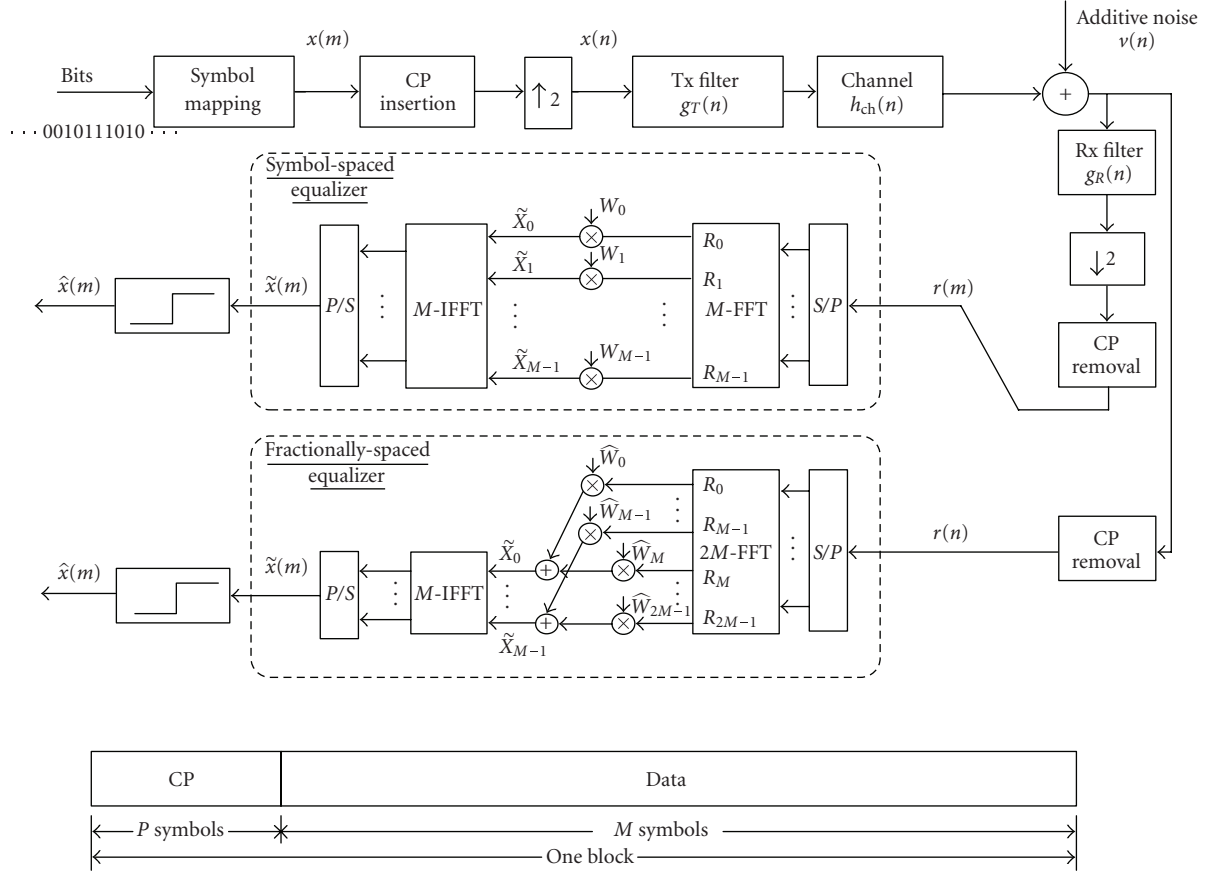
FIGURE 1: General model of FFT-SSE and FFT-FSE for single-carrier frequency-domain equalization.

### 2.1. Symbol-spaced equalizer

Suppose that $c^{SSE}(m)$ is the symbol-rate impulse response of the cascade of transmit filter $g_T(n)$, channel $h_{ch}(n)$, and receiver filter $g_R(n)$, and $C_k^{SSE}$ is the $k$th bin of its DFT transform, the DFT length being equal to the symbol block length $M$. Assuming that the length of the CP is sufficient, that is, longer than the delay spread of $c^{SSE}(n)$, we can express the $k$th subband sample as

$$R_k = C_k^{SSE}X_k + N_k, \quad k = 0, 1, \dots, M-1, \quad (2)$$

where $X_k$ is the ideal noise- and distortion-free sample and $N_k$ is zero mean Gaussian noise. The equalized frequency-domain samples are $\widetilde{X}_k = W_k R_k, k = 0, 1, \dots, M-1$. After the IFFT, the equalized time-domain signal $\widetilde{x}(m)$ is processed by a slicer to get the detected symbols $\hat{x}(m)$. The error sequence at the slicer is $e(m) = x(m) - \widetilde{x}(m)$ and MSE is defined as $E[|e(m)|^2]$.

The subband equalizer optimization criterion could be zero forcing (ZF) or MSE. In this paper, we are focusing on wideband single-carrier transmission, with heavily frequency-selective channels. In such cases, the ZF equalizers suffer from severe noise enhancement [14] and MSE provides clearly better performance. We consider here only the MSE criterion.

To minimize MSE, considering the residual intersymbol interference and additive noise, the frequency response of the optimum linear equalizer is given by [14]

$$W_k = \frac{(C_k^{SSE})^*}{|C_k^{SSE}|^2 + \sigma_n^2/\sigma_x^2}, \quad (3)$$

where $k = 0, 1, \dots, M - 1$ and $(\cdot)^*$ represents complex conjugate.

### 2.2. Fractionally-spaced equalizer

The FFT-FSE, shown in Figure 1, operates at $2\times$ symbol-rate, $2/T$. In some papers, it is also named as $T/2$-spaced equalizer [14, 18]. For each transmitted block, the received samples are processed using a $2M$-point FFT. The RRC filter block at the receiver is absent since it can be realized together with the equalizer in the frequency domain [1].

In the case of SSE, the folding is carried out before equalization, where the folding frequency is $1/2T$. It is evident in Figure 2 that uncontrolled aliasing over the transition band $F_1$ takes place. This means that SSE can only compensate for the channel distortion in the aliased received signal, which results in performance loss. On the other hand, FSE compensates for the channel distortion in received signal before the aliasing takes place. After equalization, the aliasing takes

$F_0$   Passband                $T$   Symbol duration
$F_1$   Transition band         $\alpha$   Roll-off
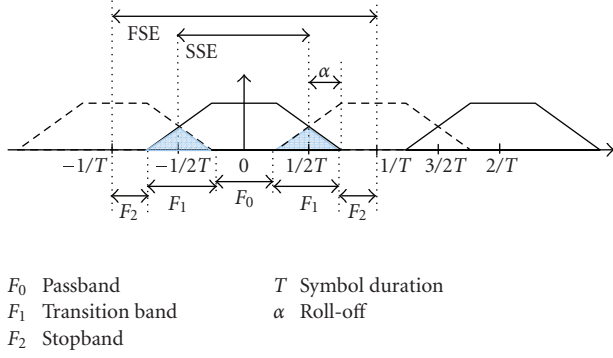$F_2$   Stopband

FIGURE 2: Signal spectra in the cases of SSE and FSE.

place in an optimal manner. The performance is expected to approach the performance of an ideal linear equalizer.

Let $H_k^{\mathrm{ch}}$, $k = 0, 1, \ldots, 2M - 1$, denote the $2M$-point DFT of the $T/2$-spaced channel impulse response, and $G_k$ denote the RRC filter in the transmitter or in the receiver side. Assuming zero-phase model for the RRC filters, $G_k$ is always real-valued. The optimum linear equalizer model includes now the following elements: transmitter RRC filter, channel $h_{\mathrm{ch}}(n)$, matched filter including receiver RRC filter and channel matched filter $h_{\mathrm{ch}}^*(-n)$, resampling at the symbol-rate, and MSE linear equalizer at symbol-rate. The $2\times$-oversampled system frequency response can be written as

$$Q_k = G_k H_k^{\mathrm{ch}} \left(H_k^{\mathrm{ch}}\right)^* G_k = \frac{\left|C_k^{\mathrm{FSE}}\right|^2}{\left(G_k\right)^2},$$
$$C_k^{\mathrm{FSE}} = H_k^{\mathrm{ch}} G_k^2. \tag{4}$$

Here $C_k^{\mathrm{FSE}}$ is the $k$th bin of DFT transform of the $T/2$-spaced impulse response of the cascade of the channel and the two RRC filters. The channel estimator described in Section 3.4 provides estimates for $C_k^{\mathrm{FSE}}$. Now the frequency bins $k$ and $M + k$ carry redundant information about the same subband data, just weighted differently by the RRC filters and the channel. The folding takes place in the sampling rate reduction, adding up these pairs of frequency bins. Before the addition, it is important to compensate the channel phase response so that the two bins are combined coherently, and also to weight the amplitudes in such a way that the SNR is maximized. The maximum ratio combining idea [1] and the sampled matched filter model [14] lead to the same result. Combining this front-end model with the MSE linear equalizer leads to the following expression for the optimal subband equalizer coefficients:

$$\widehat{W}_k = \frac{\left(C_k^{\mathrm{FSE}}\right)^* / G_k}{\left|Q_k\right| + \left|Q_{(M+k)_{\mathrm{mod}(2M)}}\right| + \sigma_n^2/\sigma_x^2}. \tag{5}$$

The frequency index $k = 0, 1, \ldots, 2M - 1$ covers the entire spectrum $[0, 2\pi]$ as $\omega_k = 2\pi k/2M$, that is, $k = 0$ corresponds to DC and $k = M$ corresponds to the symbol-rate $1/T$. It should be noted that here the equalizer coefficients imple-

ment the whole matched filter together with the MSE equalizer. The whole spectrum, where the equalization takes place, that is, the FFT frequency bins, can be grouped into three frequency regions with different equalizer actions.

(i) *Passbands $F_0$*: $k \in [0, (1 - \alpha)M/2] \cup [(3 + \alpha)M/2, 2M - 1]$.
There is no aliasing in these two regions, so the equalizer coefficients can be written in simplified form as

$$\widehat{W}_k = \frac{\left(C_k^{\mathrm{FSE}}\right)^* / G_k}{\left|Q_k\right| + \sigma_n^2/\sigma_x^2}. \tag{6}$$

(ii) *Transition bands $F_1$*: $k \in [(1 - \alpha)M/2, (1 + \alpha)M/2] \cup [(3 - \alpha)M/2, (3 + \alpha)M/2]$.
Aliasing takes place when the received signal is folded, and (5) should be used.

(iii) *Stopbands $F_2$*: $k \in [(1 + \alpha)M/2, (3 - \alpha)M/2]$.
Only noise and interference components are included and all subband signals can be set to zero, $\widehat{W}_k = 0$.

The use of oversampling provides robustness to the sampling phase. Basically the frequency-domain equalizer implements also symbol-timing adjustment. Furthermore, compared with the SSE system, the receiver filter of the FSE system can be implemented efficiently in the frequency domain. This means that the pulse shaping filtering will not introduce additional computational complexity, even if it has very sharp transition bands.

### 2.3. Computational complexity of SSE and FSE

In the following example, we will count the real multiplications at the receiver side. The complexity mainly comes from RRC filtering, FFT and IFFT, and equalization.

(i) Suppose that $M = 512$ symbols are transmitted in a block. The number of the received samples is $2M = 1024$ because of the oversampling by 2.

(ii) Each subband equalizer has only one complex weight, resulting in 4 real multiplications per subband.

(iii) The pulse shaping filter is an RRC filter with the roll-off factor of $\alpha = 0.22$ and the length of $N_{\mathrm{RRC}} = 31$. Because of symmetry, only $(N_{\mathrm{RRC}} + 1)/2 = 16$ multipliers are needed for the RRC filtering in the SSE. In an efficient decimation structure, $(N_{\mathrm{RRC}} + 1)/2$ multiplications per symbol are needed, both for the real and imaginary parts of the received signal.

(iv) The split-radix algorithm [19] is applied to the FFT. For an $M$-point FFT, $M(\log_2 M - 3) + 4$ real multiplications are needed.

(v) In the case of SSE, the total number of real multiplications per symbol is about $(N_{\mathrm{RRC}} + 1) + 2\log_2 M - 2 \approx 48$.

(vi) In the case of FSE, the number of subbands used is $M(1 + \alpha)$. The total number of real multiplications per symbol is about $3\log_2 M - 3 + 4\alpha \approx 25$.

From the above discussion, we can easily conclude that FFT-FSE has lower rate of real multiplications than FFT-SSE. This is mainly due to the reason that much of the complexity is saved when the RRC filter is realized in frequency domain.
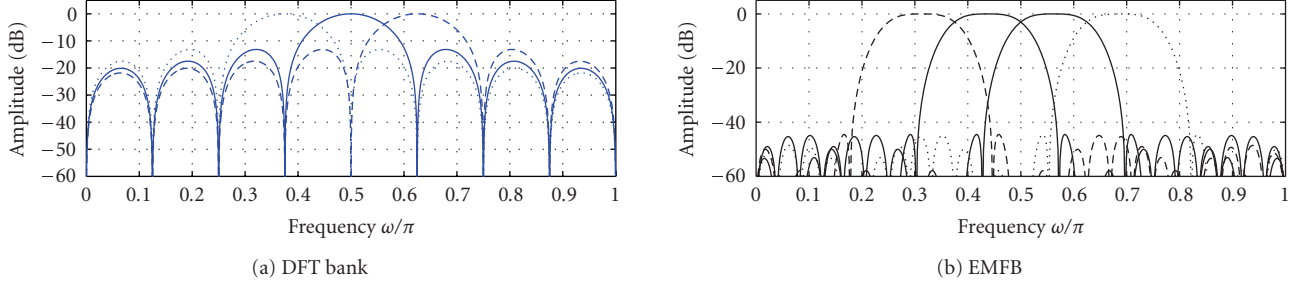
(a) DFT bank



(b) EMFB

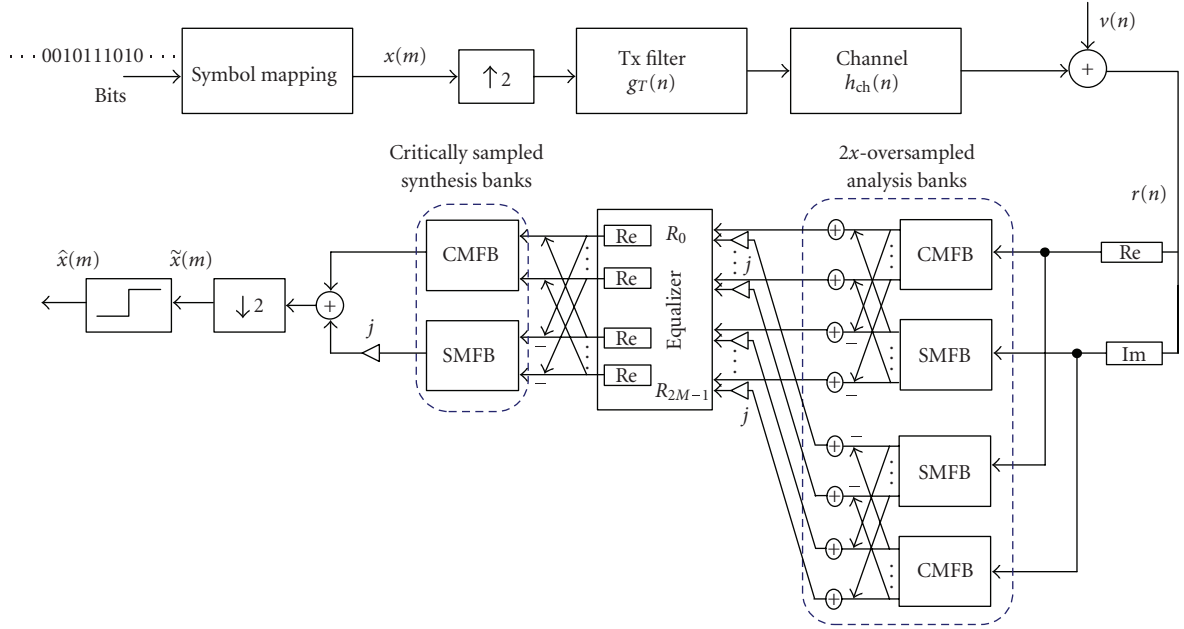FIGURE 3: Comparison of the subband frequency responses of DFT and EMFB.



FIGURE 4: Generic FB-FDE system model in the FSE case.

## 3.  EXPONENTIALLY MODULATED FILTER BANK BASED FDE

Filter banks provide an alternative way to perform the signal transforms between time and frequency domains, instead of FFT. As shown in Figure 3, exponentially modulated FBs (EMFBs) achieve better frequency selectivity than DFT banks, but they have the drawback that, since the basis functions are overlapping and longer than a symbol block, the CP cannot be utilized. Consequently, the subbands cannot be considered to have flat frequency responses. However, the lack of CPs can be considered a benefit, since CPs add overhead and reduce the spectral efficiency. Furthermore, in the FSE case, frequency-domain filtering with a filter bank is quite effective in suppressing strong interfering spectral components in the stopband regions of the RRC filter.

Figure 4 shows the FB-FSE model including a complex exponentially modulated analysis-synthesis filter bank structure as the core of frequency-domain processing. The filter bank structure has complex baseband I/Q signals as its input and output, as required for spectrally efficient radio communications. The sampling rate conversion factor in the analysis and synthesis banks is $M$, and there are $2M$ low-rate subbands equally spaced between $[0, 2\pi]$. In the critically sampled case, this FB has a real format for the low-rate subband signals [12].

### 3.1.  Exponentially modulated filter bank

EMFB belongs to a class of filter banks in which the subfilters are formed by modulating an exponential sequence with the lowpass prototype impulse response $h_p(n)$ [11, 12]. Exponential modulation translates $H_p(e^{j\omega})$ (lowpass frequency response of the prototype filter) to a new center frequency determined by the subband index $k$. The prototype filter $h_p(n)$ can be optimized in such a manner that the filter bank satisfies the perfect reconstruction condition, that is,

the output signal is purely a delayed version of the input signal. In the general form, the EMFB synthesis filters $f_k^e(n)$ and analysis filters $g_k^e(n)$ can be written as

$$f_k^e(n) = \sqrt{\frac{2}{M}} h_p(n) \exp\left(j\left(n + \frac{M+1}{2}\right)\left(k + \frac{1}{2}\right)\frac{\pi}{M}\right),$$

$$g_k^e(n) = \sqrt{\frac{2}{M}} h_p(n) \exp\left(-j\left(N_B - n + \frac{M+1}{2}\right)\left(k + \frac{1}{2}\right)\frac{\pi}{M}\right),$$

(7)

where $n = 0, 1, \ldots, N_B$ and subband index $k = 0, 1, \ldots, 2M - 1$. Furthermore, it is assumed that the subband filter order is $N_B = 2KM - 1$. The overlapping factor $K$ can be used as a design parameter because it affects how much stopband attenuation can be achieved. Another essential design parameter is the stopband edge of the prototype filter $\omega_s = (1 + \rho)\pi/2M$, where the roll-off parameter $\rho$ determines how much adjacent subbands overlap. Typically, $\rho = 1.0$ is used, in which case only the neighboring subbands are overlapping with each other, and the overall subband bandwidth is twice the subband spacing.

The amplitude responses of the analysis and synthesis filters divide the whole frequency range $[0, 2\pi]$ into equally wide passbands. EMFB has odd channel stacking, that is, $k$th subband is centered at the frequency $(k + 1/2)\pi/M$. After decimation, the even-indexed subbands have their passbands centered at $\pi/2$ and the odd-indexed at $-\pi/2$. This unsymmetry has some implications in the later formulations of the subband equalizer design.

In our approach, EMFB is implemented using cosine- and sine-modulated filter bank (CMFB/SMFB) blocks [11, 12], as can be seen in Figure 4. The extended lapped transform is an efficient method for implementing perfect reconstruction CMFBs [20] and SMFBs [21]. The relations between the $2M$-channel EMFB and the corresponding $M$-channel CMFB and SMFB with the same real prototype are

$$f_k^e(n) = \begin{cases} f_k^c(n) + j f_k^s(n), & k \in [0, M-1], \\ -(f_{2M-1-k}^c(n) - j f_{2M-1-k}^s(n)), & k \in [M, 2M-1], \end{cases}$$

$$g_k^e(n) = \begin{cases} g_k^c(n) - j g_k^s(n), & k \in [0, M-1], \\ -(g_{2M-1-k}^c(n) + j g_{2M-1-k}^s(n)), & k \in [M, 2M-1], \end{cases}$$

(8)

where $g_k^c(n)$ and $g_k^s(n)$ are the analysis CMFB/SMFB subfilter impulse responses, $f_k^c(n)$ and $f_k^s(n)$ are the synthesis bank subfilter responses (the superscript denotes the type of modulation). They can be generated according to (7).

One additional feature of the structure in Figure 4 is that, while the synthesis filter bank is critically sampled, the subband output signals of the analysis bank are oversampled by the factor of two. This is achieved by using the complex I/Q subband signals, instead of the real ones which would be sufficient for reconstructing the analysis bank input signal in the synthesis bank when no subband processing is used [10, 13] (in a critically sampled implementation, the two lower most

blocks of the analysis bank of Figure 4 would be omitted). For a block of $M$ complex input samples, $2M$ real subband samples are generated in the critically sampled case and $2M$ complex subband samples are generated in the oversampled case.

The advantage of using 2×-oversampled analysis filter bank is that the channel equalization can be done within each subband independently of the other subbands. Assuming roll-off $\rho = 1.0$ or less in the filter bank design, the complex subband signals of the analysis bank are essentially alias-free. This is because the aliasing signal components are attenuated by the stopband attenuation of the subband responses. Subband-wise equalization compensates the channel frequency response over the whole subband bandwidth, including the passband and transition bands. The imaginary parts of the subband signals are needed only for equalization. The real parts of the subband equalizer outputs are sufficient for synthesizing the time-domain equalized signal, using a critically sampled synthesis filter bank.

It should be mentioned that an alternative to oversampled subband processing is to use a critically sampled analysis bank together with subband processing algorithms that have cross-connections between the adjacent subbands [22]. However, we believe that the oversampled model results in simplified subband processing algorithms and competitive complexity.

After the synthesis bank, the time-domain symbol-rate signal is fed to the detection device. In the FSE model of Figure 4, the synthesis bank output signal is downsampled to the symbol-rate. In the case of FSE with frequency-domain folding, an $M$-channel synthesis bank would be sufficient, instead of the $2M$-channel bank. The design of such a filter bank system in the nearly perfect reconstruction sense is discussed in [23].

We consider here the use of EMFB which has odd channel stacking, that is, the center-most pair of subbands is symmetrically located around the zero frequency at the baseband. We could equally well use a modified EMFB structure [13] with even channel stacking, that is, center-most subband is located symmetrically around the zero frequency, which has a slightly more efficient implementation structure based on DFT processing. Also modified DFT filter banks [24] could be utilized with some modifications in the baseband processing. However, the following analysis is based on EMFBs since they result in the most straightforward system model.

Further, the discussion is based on the use of perfect reconstruction filter banks, but also nearly perfect reconstruction (NPR) designs could be utilized, which usually result in shorter prototype filter length. In the critically sampled case, the implementation benefits of NPR are limited, because the efficient extended lapped transform structures cannot be utilized [12]. However, in the 2×-oversampled case, having parallel CMFB and SMFB blocks, the implementation benefit of the NPR designs could be significant.

### 3.2. Channel equalizer structures and designs

In the filter bank, the number of subbands is selected in such a way that the channel is mildly frequency selective within

each individual subband. We consider here several low-complexity subband equalizers which are designed to equalize the channel optimally at a small number of selected frequency points within each subband. Figure 5 shows one example, where the subband equalizer is determined by the channel response of three selected frequency points, one at the center frequency, the other two at the subband edges. In this example, the ZF criterion is used for equalization, that is, the channel frequency response is exactly compensated at those selected frequency points.

### 3.2.1. CFIR-FBEQ

A very basic approach is to use a complex FIR filter as a subband equalizer. A 3-tap FIR filter,[1] $E^{\mathrm{CFIR}}(z) = c_0 z + c_1 + c_2 z^{-1}$, has the required degrees of freedom to equalize the channel frequency response within each subband.

It should be noted that the subband equalizer response depends on the number of frequency points considered within each subband. Regarding the choice of the specific frequency points, the design can be greatly simplified when the choice is among the normalized frequencies $\omega = 0, \pm\pi/2$, and $\pm\pi$. At the selected frequency points, the equalizer is designed to take the target values given by (5) in the FSE case and by (3) in the SSE case. Below we focus on the MSE based FSE.

When three subband frequency points are selected in the subband equalizer design, there are a total of $4M$ frequency points for $2M$ subbands, that is, we consider the MSE equalizer response $\widehat{W}_\kappa$ at equally spaced frequency points $\kappa\pi/(2M)$, $\kappa = 0, 1, \ldots, 4M - 1$. For notational convenience, we define the target frequency responses in terms of subband index $k = 0, 1, \ldots, 2M - 1$, instead of frequency point index $\kappa$. The $k$th subband target response value is denoted as $\eta_{ik}$, which is defined as

$$\eta_{ik} = \widehat{W}_{2k+i}, \quad i = 0, 1, 2. \tag{9}$$

At the low rate after decimation, these frequency points $\{\eta_{0k}, \eta_{1k}, \eta_{2k}\}$ are located for the even subbands at the normalized frequencies $\omega = \{0, \pi/2, \pi\}$, and for the odd subbands at the frequencies $\omega = \{-\pi, -\pi/2, 0\}$. Combining (5) and (9), we can get the following equations for the subband equalizer response $E^{\mathrm{CFIR}}(e^{j\omega})$ at these target frequencies.

Even subbands:

$$E_k^{\mathrm{CFIR}}(e^{j\omega}) = \begin{cases} c_{0k} + c_{1k} + c_{2k} = \eta_{0k}, & (\omega = 0), \\ jc_{0k} + c_{1k} - jc_{2k} = \eta_{1k}, & \left(\omega = \dfrac{\pi}{2}\right), \\ -c_{0k} + c_{1k} - c_{2k} = \eta_{2k}, & (\omega = \pi). \end{cases} \tag{10}$$

Odd subbands:

$$E_k^{\mathrm{CFIR}}(e^{j\omega}) = \begin{cases} -c_{0k} + c_{1k} - c_{2k} = \eta_{0k}, & (\omega = -\pi), \\ -jc_{0k} + c_{1k} + jc_{2k} = \eta_{1k}, & \left(\omega = \dfrac{-\pi}{2}\right), \\ c_{0k} + c_{1k} + c_{2k} = \eta_{2k}, & (\omega = 0). \end{cases} \tag{11}$$



(a) Amplitude compensation



(b) Phase compensation

FIGURE 5: An example of AP-FBEQ subband equalizer responses.

---

[1] In practice, the filter is realized in the causal form $z^{-1}E^{\mathrm{CFIR}}(z)$.
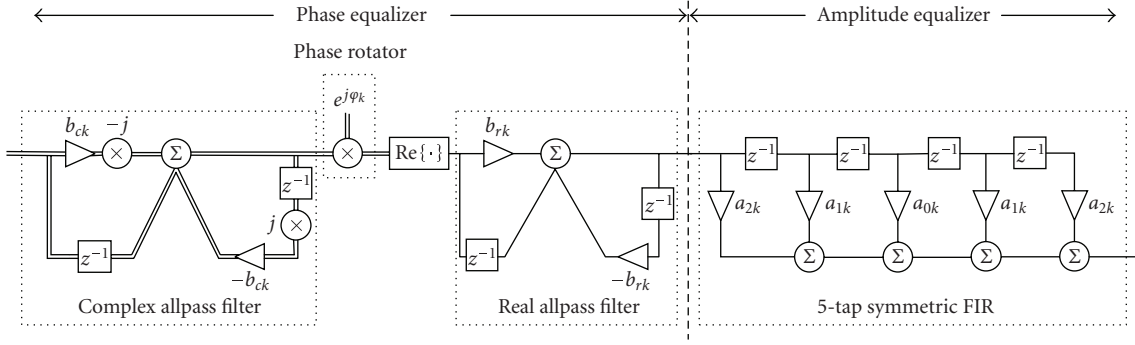
FIGURE 6: An example of the AP-FBEQ subband equalizer structure.

The 3-tap complex FIR coefficients $\{c_{0k}, c_{1k}, c_{2k}\}$ of the $k$th subband equalizer can be obtained as follows (+ signs stand for even subbands and − signs for odd subbands, resp.):

$$c_{0k} = \pm\frac{1}{2}\left(\frac{\eta_{0k} - \eta_{2k}}{2} - j\left(\eta_{1k} - \frac{\eta_{0k} + \eta_{2k}}{2}\right)\right),$$

$$c_{1k} = \frac{\eta_{0k} + \eta_{2k}}{2}, \tag{12}$$

$$c_{2k} = \pm\frac{1}{2}\left(\frac{\eta_{0k} - \eta_{2k}}{2} + j\left(\eta_{1k} - \frac{\eta_{0k} + \eta_{2k}}{2}\right)\right).$$

### 3.2.2. AP-FBEQ

The idea of AP-FBEQ approach is to compensate channel amplitude and phase distortion separately. In other words, at those selected frequency points, the amplitude response of the equalizer is proportional to the inverse of the channel amplitude response, and the phase response of the equalizer is the negative of the channel phase response.

The subband equalizer structure, shown in Figure 6, is a cascade of a phase equalization section, consisting of allpass filter stages and a phase rotator, and an amplitude equalization section, consisting of a linear-phase FIR filter. This particular structure makes it possible to design the amplitude equalization and phase equalization independently, leading to simple formulas for channel estimation based solutions, or simplified and fast adaptive algorithms for adaptive subband equalizers. In this paper, we refer to this frequency-domain equalization approach as the amplitude-phase filter bank equalizer, AP-FBEQ.

The real parts of the equalized subband signals are sufficient for constructing the sample sequence for detection, and the imaginary parts are irrelevant after the subband equalizers. In the basic form of the AP-FBEQ subband equalizer, the operation of taking the real part would be after all the filters of the subband equalizer. But since the real filters (real allpass and magnitude equalizer) act independently on the real (I) and imaginary (Q) branch signals, the results of the Q-branch computations after the phase rotator would never be utilized. Therefore, it is possible to move the real part operation and combine it with the phase rotator, that is,

only the real part of the phase rotator output needs to be calculated, and the real filters are implemented only for the I-branch. The structure of Figure 6 is completely equivalent with the original one, but it is computationally much more efficient. With the same kind of reasoning, it is easy to see that in the CFIR-FBEQ case, only two real multipliers are needed to implement each of the taps.

The orders of the equalizer sections, as well as the number of specific frequency points used in the subband equalizer design, offer a degree of freedom and are chosen to obtain a low-complexity solution. Firstly, we consider the subband equalizer structure shown in Figure 6. The transfer functions of the complex and real first-order allpass filters $A_k^c(z)$ and $A_k^r(z)$ can be given by[2]

$$A_k^c(z) = \frac{1 - jb_{ck}z}{1 + jb_{ck}z^{-1}},$$

$$A_k^r(z) = \frac{1 + b_{rk}z}{1 + b_{rk}z^{-1}}, \tag{13}$$

respectively. The phase response of the equalizer for the $k$th subband can be described as

$$\begin{aligned}
\arg\left[E_k^{\mathrm{AP}}(e^{j\omega})\right] &= \arg\left(e^{j\varphi_k} \cdot A_k^c(e^{j\omega}) \cdot A_k^r(e^{j\omega})\right) \\
&= \varphi_k + 2\arctan\left(\frac{-b_{ck}\cos\omega}{1 + b_{ck}\sin\omega}\right) \\
&\quad + 2\arctan\left(\frac{b_{rk}\cos\omega}{1 + b_{rk}\sin\omega}\right).
\end{aligned} \tag{14}$$

The equalizer magnitude response for the $k$th subband can be written as

$$\left|E_k^{\mathrm{AP}}(e^{j\omega})\right| = \left|a_{0k} + 2a_{1k}\cos\omega + 2a_{2k}\cos 2\omega\right|. \tag{15}$$

The AP-FBEQ idea can be applied to both SSE and FSE in similar manner as CFIR-FBEQ. Here, we focus on the FSE case. Three subband frequency points at normalized frequencies $\omega = \{0, \pi/2, \pi\}$ for the even subbands and $\omega = \{-\pi, -\pi/2, 0\}$ for the odd subbands are selected in the subband equalizer design. Here, we define the target amplitude

---

[2] The allpass filters can be realized in the causal form $z^{-1}A_k(z)$.

and phase response values for subband $k$ as $\epsilon_{ik}$ and $\zeta_{ik}$, respectively:

$$\begin{aligned} \epsilon_{ik} &= |\widehat{W}_{2k+i}|, \\ \zeta_{ik} &= \arg(\widehat{W}_{2k+i}), \quad i = 0, 1, 2. \end{aligned} \tag{16}$$

Then, combining (5), (14), (15), and (16) at these target frequencies, we can derive two allpass filter coefficients $\{b_{ck}, b_{rk}\}$ and a phase rotator $\varphi_k$ for phase compensation section and the FIR coefficients $\{a_{0k}, a_{1k}, a_{2k}\}$ for amplitude compensation.

In this paper, the following three different low-complexity designs of the AP-FBEQ structure are considered. (+ signs stand for the even subbands and − signs for the odd ones.)

*Case 1.* One frequency point is selected in the subband. This model of subband equalizer consists only of the phase rotator $e^{j\varphi_k}$ for phase compensation and a real coefficient $a_{0k}$ for amplitude compensation. In fact, it behaves like one complex equalizer coefficient for each subband in the FFT-FDE system. The subband center frequency point is selected to determine the equalizer response

$$\varphi_k = \zeta_{1k}, \qquad a_{0k} = \epsilon_{1k}. \tag{17}$$

*Case 2.* Two frequency points are selected at the subband edges at the frequency points $\omega = 0$ and $\pm\pi$ to determine the equalizer coefficients. The subband equalizer structure consists of a cascade of a first-order complex allpass filter followed by a phase rotator and an operation of taking the real part of the signal. Finally, a symmetric linear-phase 3-tap FIR filter is applied for amplitude compensation. In this case, the equalizer coefficients can be calculated as

$$\begin{aligned} \varphi_k &= \frac{\zeta_{0k} + \zeta_{2k}}{2}, & a_{0k} &= \frac{1}{2}(\epsilon_{0k} + \epsilon_{2k}), \\ b_{ck} &= \pm\tan\left(\frac{\zeta_{2k} - \zeta_{0k}}{4}\right), & a_{2k} &= \pm\frac{1}{4}(\epsilon_{0k} - \epsilon_{2k}). \end{aligned} \tag{18}$$

*Case 3.* Three frequency points are used in each subband, as we have discussed above, one at the subband center and two at the passband edges. The equalizer structure contains two allpass filters, a phase rotation stage and a symmetric linear-phase 5-tap FIR filter. Their coefficients are calculated as below:

$$\begin{aligned} \varphi_k &= \frac{\zeta_{0k} + \zeta_{2k}}{2}, & a_{0k} &= \frac{\epsilon_{0k} + 2\epsilon_{1k} + \epsilon_{2k}}{4}, \\ b_{ck} &= \pm\tan\left(\frac{\zeta_{2k} - \zeta_{0k}}{4}\right), & a_{1k} &= \pm\left(\frac{\epsilon_{0k} - \epsilon_{2k}}{4}\right), \\ b_{rk} &= \pm\tan\left(\frac{\zeta_{1k} - \varphi_k}{2}\right), & a_{2k} &= \pm\left(\frac{\epsilon_{0k} - 2\epsilon_{1k} + \epsilon_{2k}}{8}\right). \end{aligned} \tag{19}$$

The subband equalizer structure is not necessarily fixed in advance but can be determined individually for each subband based on the frequency-domain channel estimates. This enables the structure of each subband equalizer to be controlled such that each subband response is equalized optimally at the minimum number of frequency points which can be expected to result in sufficient performance.

The performances of these three different subband equalizer designs, together with the 3-tap CFIR-FBEQ, will be examined in the next section.

### 3.3. FSE and SSE

Also in the SSE version of CFIR-FBEQ and AP-FBEQ, the decimating RRC filtering needs to be carried out before equalization, and uncontrolled aliasing results in similar performance loss as in the FFT-SSE.

In the FSE, the receiver RRC filter can again be implemented in the frequency domain together with the equalizer, with low complexity. Since no guard interval is employed and the subbands are highly frequency selective, frequency-domain filtering can be implemented independently of the roll-off and other filtering requirements, as long as the stopband attenuation in the filter bank design is sufficient for the receiver filter from the RF point of view. It can be noted that the FB-FSE structure provides a flexible solution for channel equalization and channel filtering, since the receiver filter bandwidth and roll-off can be controlled by adjusting the RRC-filtering part of the equalizer coefficient calculations.

In advanced receiver designs, a high initial sampling rate is often utilized, followed by a multistage decimation filter chain which is highly optimized for low-implementation complexity [25]. The first stages of the decimation chain often utilize multiplier-free structures, like the cascaded integrator comb, and the major part of the implementation complexity is at the last stage. In such designs, FB-FSE provides a flexible generic solution for the last stage of a channel filtering chain.

### 3.4. Channel estimation

FB-FDEs, as well as FFT-FDEs, can be implemented by using adaptive channel equalization algorithms to adjust the equalizer coefficients. However, we focus here on channel estimation based approach, where the equalizer coefficients are calculated at regular intervals based on the channel estimates and knowledge of the desired receiver filter frequency response, according to (3) or (5). In the performance studies, we have utilized a basic, maximum likelihood (ML) channel estimation method (also known as the least-squares method) using training sequences [26]. Here, Gold codes [27] of different lengths are used as training sequences.

In SSE, a training sequence is transmitted, and the symbol-rate channel impulse response (including transmitter and receiver RRC filters) is estimated based on the received training sequence at the decimating RRC filter output. This channel estimate is used for calculating the equalizer coefficients using (3).

In FSE, we have chosen to estimate $T/2$-spaced impulse responses (including the two RRC filters). Including the receiver RRC filter in the estimated response minimizes the noise and interference coming into the channel estimator. Now, the channel estimator utilizes the receiver RRC filter output at two times the symbol-rate. It must be noted that this approach requires a time-domain RRC filter for the training sequences in the receiver, even if frequency-domain filtering is applied to the data symbols.

## 4. NUMERICAL RESULTS

### 4.1. Basic simulations and numerical comparisons

The considered models of FFT-FDE and FB-FDE were introduced in Figures 1 and 4, respectively. The pulse shaping filters both in the transmitter and receiver are real-valued RRC filters with $\alpha = 0.22$. In the FSE case, the receiver RRC filter is realized by the equalizer. The filter bank designs in the simulations used roll-off $\rho = 1.0$, different numbers of subbands $2M = \{128, 256\}$ and overlapping factors $K = \{2, 3, 5\}$, resulting in about 30 dB, 38 dB, and 50 dB stopband attenuations, respectively.

The performances were tested using the extended vehicular-A channel model of ITU-R with the maximum excess delay of about 2.5 $\mu$s [28]. The symbol-rate was $1/T = 15.36$ MHz. The channel fading was modelled quasistatic, that is, the channel frequency response was time invariant during each frame transmission. 4000 independent channel instances were simulated to obtain the average performance. The MSE criterion was applied to solve the equalizer coefficients. The bit-error-rate (BER) performance was simulated with QPSK, 16-QAM, and 64-QAM modulations, with gray coding, and was compared to the performance of FFT-FDE. In all FFT-FDE simulations, the CP is included and assumed to be longer than the delay spread. Also the performance of the ideal MSE linear equalizer is included for reference. This analytic performance reference was obtained by applying the MSE formula for the infinite-length linear MSE equalizer from [14] and then using the well-known formulas of the Q-function and gray-coding assumption for estimating the BER. The BER measure is averaged over 5000 independent channel instances. Ideal channel estimation was assumed in Figures 7, 8, and 9, but in Figures 10, 11, and 12, the channel estimator described in Section 3.4 was utilized. The BER and frame-error-rate (FER) performance with low density parity check (LDPC) [29] error correction coding are presented in Figures 11 and 12.

### Raw BER performance of FB-FSE

Figure 7 presents the uncoded BER performance of the CFIR-FBEQ and AP-FBEQ compared to the analytic performance with QPSK, 16-QAM, and 64-QAM modulations. The three different designs of AP-FBEQ and a 3-tap CFIR-FBEQ were examined. It can be seen that the CFIR-FBEQ and AP-FBEQ Case 3 performances are rather similar, however,

with a minor but consistent benefit for AP-FBEQ. With a low number of subbands and with high-order modulation, the differences are more visible. In the following comparisons, AP-FBEQ performance is considered. It is clearly visible that AP-FBEQ Cases 2 and 3 equalizers improve the performance significantly compared to Case 1. When the modulation order becomes higher, the performance gaps between different equalizer structures increase. As the most interesting uncoded BER region is between 1% and 10%, it is seen that 256 subbands with Case 3 are sufficient to achieve good performance even with high-order modulation. The resulting performance is rather close to the analytic BER bound; however, it is clear that the gray-coding assumption is not very accurate at low $E_b/N_0$, and the analytic performance curve is somewhat optimistic. With this specific channel model, 128 subbands are sufficient for QPSK and 16-QAM modulations when AP-FBEQ Case 3 equalizer is used.

The FB design parameter, overlapping factor $K$, controls the level of stopband attenuation. Increasing $K$ improves the stopband attenuation, with the cost of increased implementation complexity. Figure 8 presents the BER performance of Case 3 equalizer with 256 subbands and the different $K$-factors. For QPSK modulation, it can be seen that the $K$-factor has relatively small effect on the performance, and even $K = 2$ may provide sufficient performance. In the case of higher order modulations, $K = 3$ can achieve sufficient performance.

### SSE versus FSE performance and FFT-FDE versus FB-FDE comparisons

Figure 9 presents the results for SSE and FSE in the FFT-FDE and FB-FDE receivers. It is clearly seen that FSE provides significant performance gain over SSE in the considered case. The performance differences between AP-FBEQ and the conventional FFT-FDE methods are relatively small. However, it should be noted that in Figure 9 the guard-interval overhead is not taken into account in the $E_b/N_0$-axis scaling, even though sufficiently long CP (200 samples) is utilized. In practice, the CP length effects in the BER plots only on the $E_b/N_0$-axis scaling.

### Guard-interval considerations

For example, 10% or 25% guard-interval length would mean about 0.4 dB or 1 dB degradation on the $E_b/N_0$-axis, respectively. The delay spread of the channel model corresponds to about 39 symbol-rate samples or 77 samples at twice the symbol-rate. Then the minimum FFT size to reach 10% guard-interval overhead is about 350 for SSE and 700 for FSE. However, the RRC pulse shaping and baseband channel filtering extend the delay spread, possibly by a factor 2, so the CP length should be in the order of 5 $\mu$s in this example. Then the practical FFT length could be 512 or 1024 for SSE and 1024 or 2048 for FSE. The conclusion is that considerably higher number of subbands is needed in the FFT case to reach realistic CP overhead.
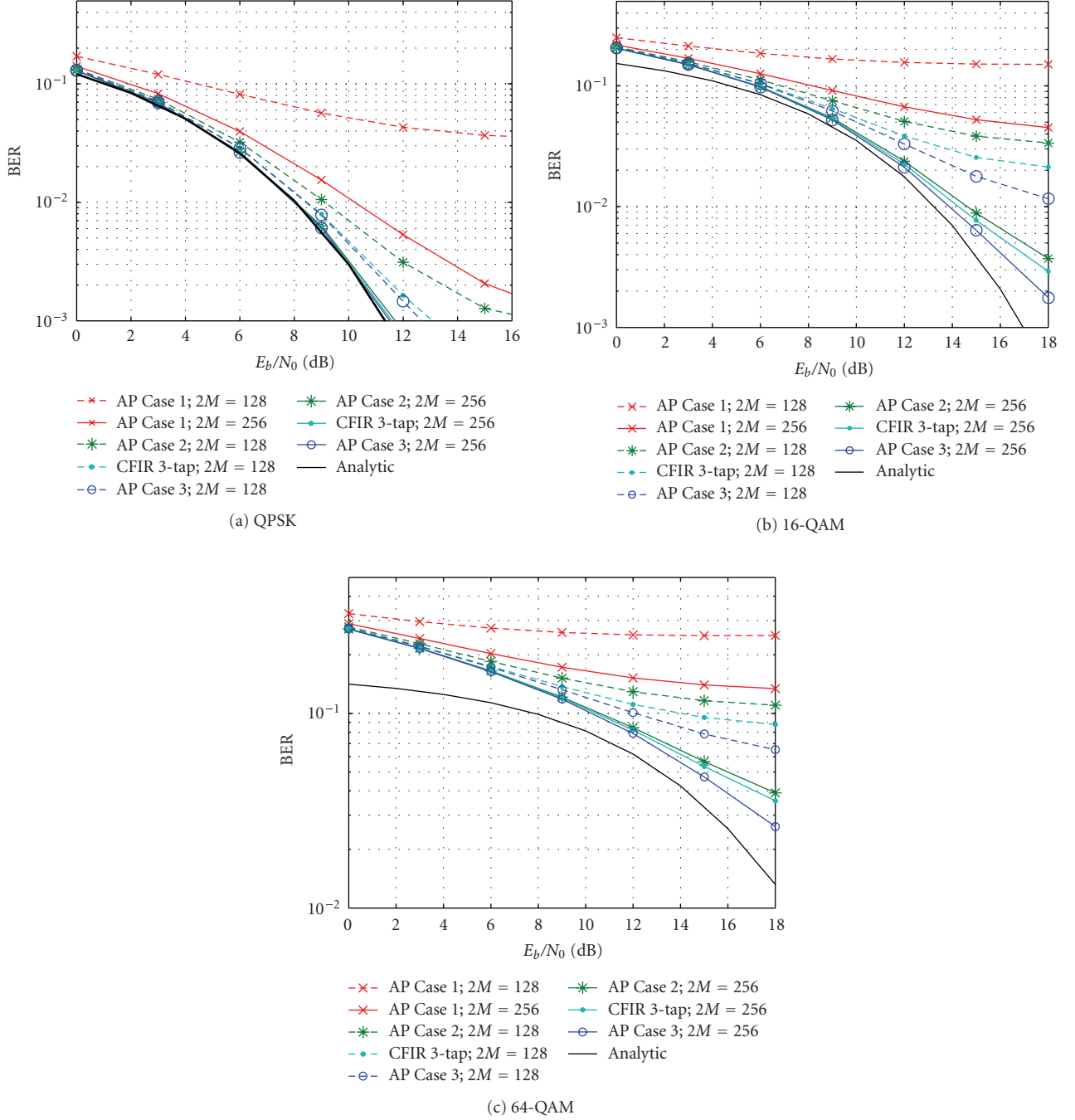
(a) QPSK



(b) 16-QAM



(c) 64-QAM

FIGURE 7: Uncoded BER performance of FB-FSE (CFIR-FBEQ 3-tap and AP-FBEQ Cases 1, 2, 3) with overlapping factor $K = 5$ and $2M = \{128, 256\}$ subbands.

*Performance with channel estimation*

In Figure 10, the uncoded BER performance of AP-FBEQ is simulated with a practical channel estimator. The channel estimator described in Section 3.4 is utilized, using Gold codes of different lengths as a training sequence. It is observed that the training sequence length of 384 symbols is quite sufficient.

## 4.2. Performance comparison with practical parameters and error-correction coding

Here, we include LDPC forward error correction (FEC) coding and the channel estimator in the simulation model. The main parameters are indicated in Table 1. With the chosen parameters, the training symbol overhead is 10% and the two systems with different LDPC code-rates transmit
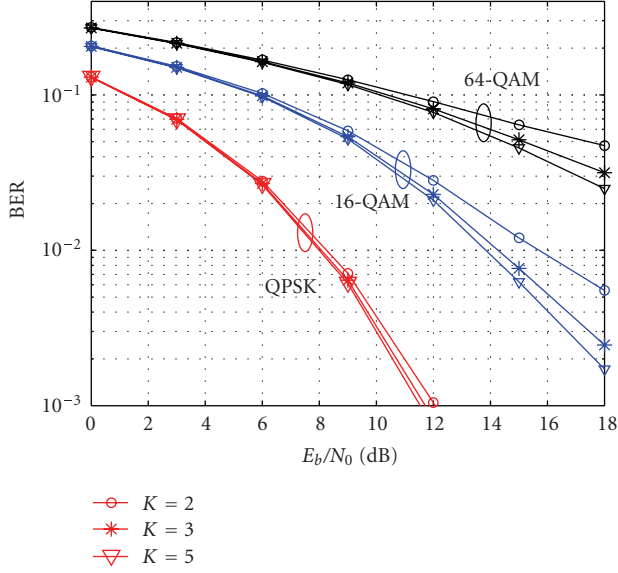
FIGURE 8: Uncoded BER performance for FB-FSE (AP-FBEQ Case 3 equalizer) with $2M = 256$ subbands and different $K$-factors.
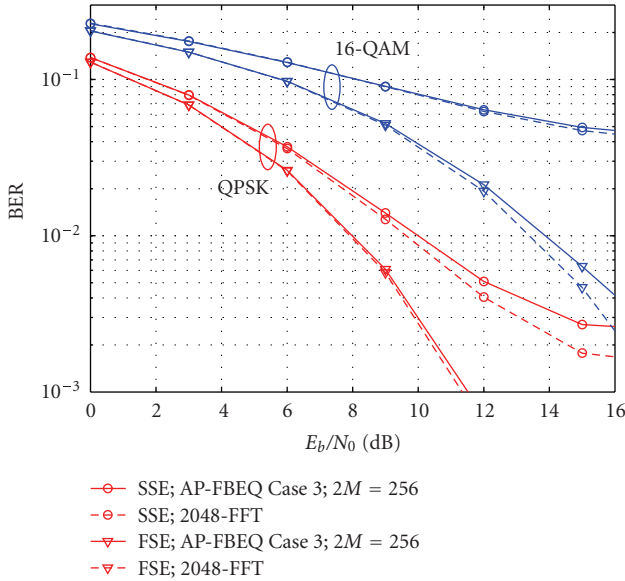


FIGURE 9: Uncoded BER performance comparison between SSE and FSE-type FB-FDE and FFT-FDE with QPSK and 16-QAM modulations. AP-FBEQ Case 3 equalizer with $2M = 256$ subbands and overlapping factor $K = 5$ was used.
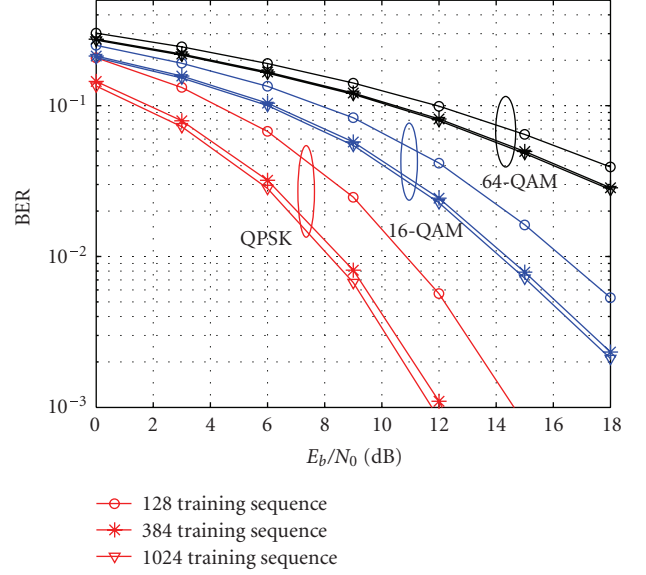


FIGURE 10: Uncoded BER performance for FB-FSE with ML based channel estimation using different training sequence lengths with QPSK, 16-QAM, and 64-QAM modulations. AP-FBEQ Case 3 equalizer with $2M = 256$ subbands and overlapping factor $K = 5$ was used.

The AP-FBEQ and CFIR-FBEQ systems are also compared in Figure 12 with the FBMC and OFDM systems of [15]. The parameters of FB-FDE are the same as in Table 1, except that code-rate 3/4 is used to reach similar bits rate with the other systems. The parameters are consistent with the ones considered in [15], with similar overhead for training sequences/pilots, signal bandwidth, and bit rates. The same type of LDPC code is used, however with higher code-rate 3/4 in OFDM and FB-FDE, and code-rate 2/3 in the FBMC system. Higher code-rate is needed in OFDM to accomodate the CP-overhead and FB-FDE to accommodate the overhead due to the excess band. With QPSK modulation, the number of source bits in one $250\,\mu$s frame are 5022, 5184, and 5320 for OFDM, FB-FDE, and FBMC, respectively.

Figure 12 displays that with QPSK modulation, FB-FDE has clear performance benefit over FBMC and CP-OFDM; whereas with 16-QAM modulation, FB-FDE and CP-OFDM are rather similar and clearly worse than that of FBMC.

### 4.3. Complexity comparison between FFT-FDEs and FB-FDEs

Here we evaluate the receiver complexity of FFT-FDEs and FB-FDEs in terms of real multiplications per detected symbol. The complexity metric includes the FB or FFT transform, subband equalizers, as well as the baseband filtering in the SSE case. The time-domain RRC filter is assumed to be of length $N_{RRC} = 31$. The receiver RRC filtering and decimation are realized in the frequency domain in both FSE systems, using half-sized IFFT or FB on the synthesis side. The split-radix algorithm [19] is applied for FFT/IFFT, critically sampled filter banks are implemented with the fast extended

exactly the same number of source bits per frame. Higher code-rate is needed in the FFT-FDE system to accommodate the CP overhead. Meanwhile, the CP length which is 1/8 of the useful symbol duration introduces $E_b/N_0$ degradation of $10\log_{10}(9/8)$ dB. The comparison of Figure 11 shows that FB-FDE has about 1 dB performance advantage over the FFT-FDE under the most interesting coded FER region 1%–10%. This is the joint results of using lower code-rate and the absence of CP $E_b/N_0$ degradation. Moreover, we can see that AP-FBEQ and CFIR-FBEQ have very similar performance.

TABLE 1: FFT-FDE and FB-FDE system parameters.

| | FB-FSE | | | FFT-FSE | | |
|---|---|---|---|---|---|---|
| Sampling rate | 30.72 MHz | | | 30.72 MHz | | |
| symbol-rate | 15.36 MHz | | | 15.36 MHz | | |
| RRC roll-off | 0.22 | | | 0.22 | | |
| Signal bandwidth | 18.74 MHz | | | 18.74 MHz | | |
| No. of subbands | 256 | | | 1024 | | |
| Data symbols per frame | 3456 | | | 3072 | | |
| Cyclic prefix (symbols) | 0 | | | 64 | | |
| Training symbols | 384 | | | 384 | | |
| Total symbols | 3840 | | | 3840 | | |
| Frame duration | 250 $\mu$s | | | 250 $\mu$s | | |
| FEC | LDPC code-rate 2/3 | | | LDPC code-rate 3/4 | | |
| Modulation | QPSK | 16-QAM | 64-QAM | QPSK | 16-QAM | 64-QAM |
| Transmit bits (coded) | 6912 | 13824 | 20736 | 6144 | 12288 | 18432 |
| Source bits | 4608 | 9216 | 13824 | 4608 | 9216 | 13824 |

TABLE 2: Receiver complexity comparison between the FB-FDE and FFT-FDE receivers: number of real multiplications per symbol.

| FFT-FDE | | $M = 1024$ | $M = 2048$ |
|---|---|---|---|
| SSE | $2\log_2 M - 4 + (N_{\text{RRC}} + 1)$ | 48 | 50 |
| FSE | $3\log_2 M - 6 + 4\alpha$ | 24 | 27 |
| FSE with time-domain RRC | $3\log_2 M - 6 + 4\alpha + 2(N_{\text{RRC}} + 1)$ | 88 | 91 |
| FB-FDE | | $M = 128; K = 2$ | $M = 256; K = 5$ |
| (1) *AP-FBEQ* | | | |
| SSE, Case 1 | $6K + 3\log_2 M - 1 + N_{\text{RRC}}$ | 63 | 84 |
| SSE, Case 2 | $6K + 3\log_2 M + 2 + N_{\text{RRC}}$ | 66 | 87 |
| SSE, Case 3 | $6K + 3\log_2 M + 4 + N_{\text{RRC}}$ | 68 | 89 |
| FSE, Case 1 | $10K + 5\log_2 M - 4 + 2\alpha$ | 51 | 86 |
| FSE, Case 2 | $10K + 5\log_2 M - 1 + 5\alpha$ | 55 | 90 |
| FSE, Case 3 | $10K + 5\log_2 M + 1 + 7\alpha$ | 57 | 92 |
| (2) *CFIR-FBEQ* | | | |
| FSE, 3-taps | $10K + 5\log_2 M + 6\alpha$ | 56 | 91 |

lapped transform algorithm [12], and the oversampled analysis banks are implemented using the optimized FFT based structure of [13]. The needed number of real multiplications for a block of $M$ high-rate samples is $M(\log_2 M - 3) + 4$ for the FFT or IFFT, $M(2K + \log_2 M + 2)$ for the critically sampled synthesis bank, and $2M(2K + \log_2 M - 2)$ for an oversampled analysis bank. For FB-FDE, we have seen that 128 or 256 subbands are sufficient, whereas 1 k or 2 k FFT lengths are required. For FB-FDE, 2 real multipliers are needed for each tap of the CFIR, 2 for the first-order complex allpass and 1 for the real allpass (the two multipliers in the allpass structures of Figure 6 can be combined), two for phase rotation, and 2 for amplitude equalizer (we can scale $a_0 = 1$, and do the overall signal scaling in the phase rotator). The overall complexity figures are shown in Table 2, considering two extreme cases of filter bank complexity.

The comparison between SSE and FSE depends very much on the needed baseband RRC and channel filter complexity, but it is evident that, also in the FB-FDE case, FSE may actually be less complex to implement than SSE. The complexity of FB-FDE depends heavily on the $K$ factor of the FB design. The subband equalizer choice has a minor effect on the overall complexity.

In a CP based system, the capability of the frequency-domain filter to suppress strong adjacent channels or other interferences in the stopbands are limited due to FFT blocking effects. Assume that there is a strong interference signal in the stopband of the RRC filter. Removing the CPs would cause transients in the interference waveforms, and these would cause relatively strong error transients at the ends of the time-domain symbol blocks even after filtering. Thus it seems that a baseband filter before the FFT is needed in CP based single-carrier FDE. FB-FSE may actually be very competitive compared to FFT-FSE, if additional baseband filtering is needed in the latter structure. With oversampled equalizer processing, the implementation of the baseband filter is not as efficient as in the SSE case. In the example setup, if the RRC filter is implemented in time-domain at 2× symbol-rate, the FFT-FSE multiplication rates are increased by 64 multiplications per symbol.
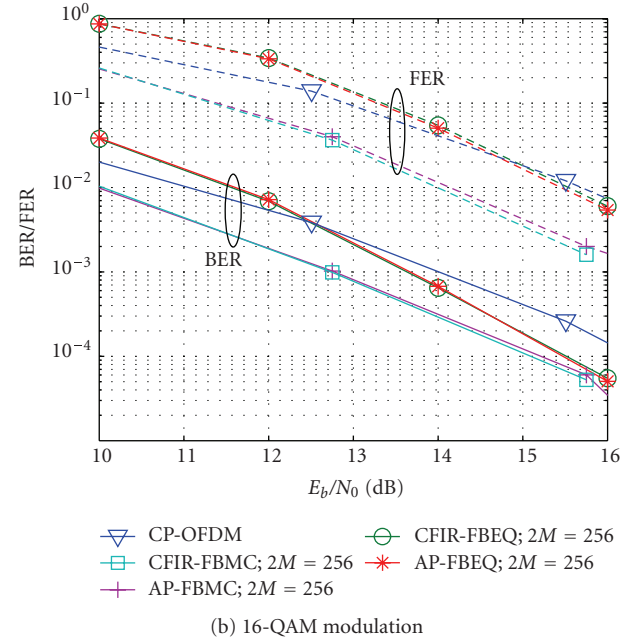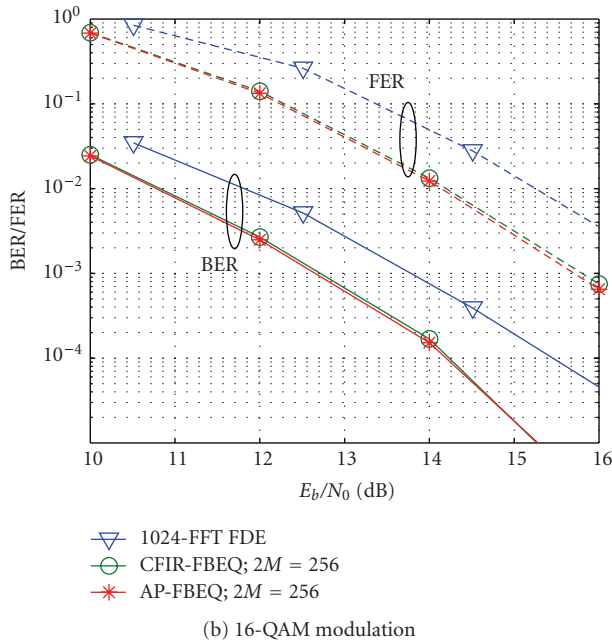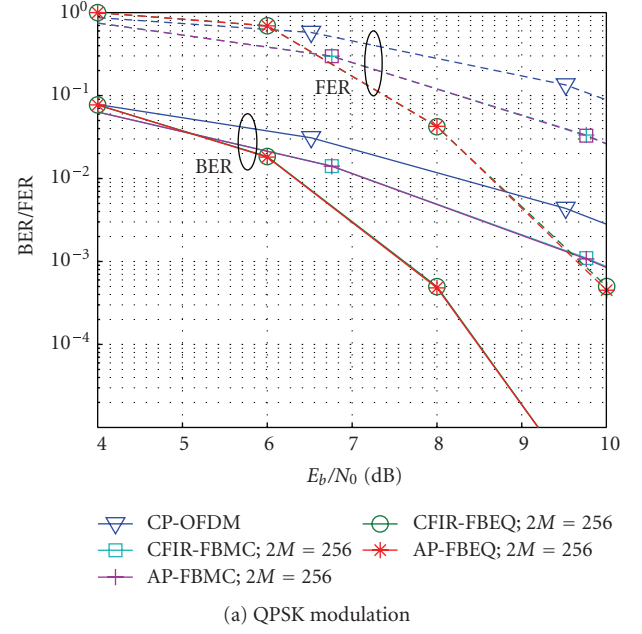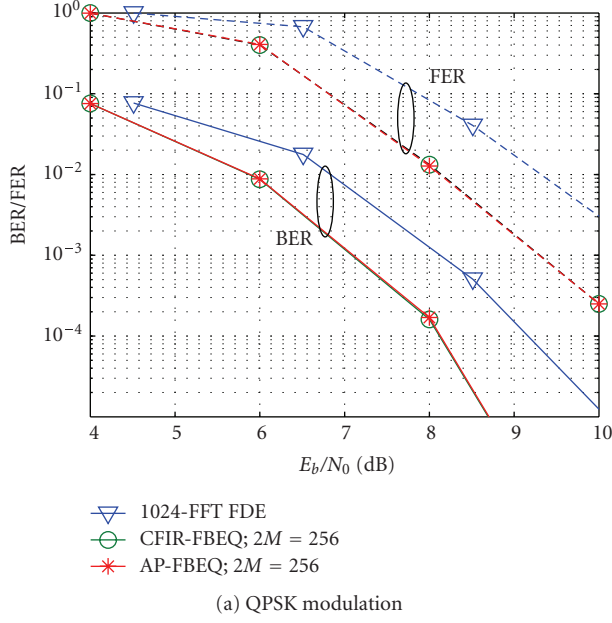
(a) QPSK modulation



(b) 16-QAM modulation

FIGURE 11: Coded BER and FER performance comparison between FFT-FSE and FB-FSE with practical system parameters and LDPC coding. Both 3-tap CFIR and AP Case 3 subband equalizers are included in FB-FSE models.



(a) QPSK modulation



(b) 16-QAM modulation

FIGURE 12: Coded BER and FER performance comparison between CP-OFDM, FBMC, and FB-FSE with practical system parameters and LDPC coding. Both 3-tap CFIR and AP Case 3 subband equalizers are included in FBMC and FB-FSE models.

## 5.  CONCLUSION

We have presented a filter bank based frequency-domain equalizer with mildly frequency-selective subband processing and a modest number of subbands. The performance is better than that of the FFT-FDE. Furthermore, FB-FDE is applicable to any single carrier system, whether CP is included or not.

In certain wireless communication scenarios, strong narrowband interferences (NBI) are considered as a serious problem [30], and various methods have been developed for mitigating their effects. Frequency-domain NBI mitigation can be easily combined with both FFT-FDE and FB-FDE with minor additional complexity. It has been observed that FFT based frequency-domain filtering has limitations as NBI mitigation method due to the FFT leakage, while filter bank based approaches provide clearly better performance [30–32].

Regarding the choice between CFIR-FBEQ and AP-FBEQ, it was seen that the latter gives consistently slightly better performance with the cost of slightly higher multiplication rate. Furthermore, in AP-FBEQ, the amplitude and phase responses can be adjusted independently of each other, which is a very useful feature in many respects. For example, in [33] the equalizer amplitude response is tuned to enhance narrowband interference suppression. In [23], a filter bank system with a $2M$-channel analysis bank and an $M$-channel synthesis bank is developed, and it is observed that tuning of the phase response in the subband equalizers is needed to achieve nearly perfect reconstruction characteristics with low distortion.

The overlapped-FFT algorithms also avoid the use of CPs. This structure can be seen as a kind of a simple filter bank with basis functions overlapping in time [7–9]. It can be seen that there is a continuum of filter bank design cases between the overlapped FFT based approach and the FB based designs with high $K$ values. If the frequency selectivity of the filter bank design is not important, then relatively low-complexity designs probably provide the best tradeoff. As we have seen, the performance difference between $K = 3$ and $K = 5$ is relatively small.

The complexity of FB-FDEs is no doubt higher than that of FFT-FDE structures. However, we believe that the same filter bank can be used to implement part of the channel filtering, with much higher performance than when using the FFT-FDE structures. FB-FDE provides an easily configurable structure for the final stage of the channel filtering chain, together with the channel equalization functionality.

## REFERENCES

[1] M. V. Clark, "Adaptive frequency-domain equalization and diversity combining for broadband wireless communications," *IEEE Journal on Selected Areas in Communications*, vol. 16, no. 8, pp. 1385–1395, 1998.

[2] G. Kadel, "Diversity and equalization in frequency domain - a robust and flexible receiver technology for broadband mobile communication systems," in *Proceedings of IEEE 47th Vehicular Technology Conference (VTC '97)*, vol. 2, pp. 894–898, Phoenix, Ariz, USA, May 1997.

[3] D. Falconer, S. L. Ariyavisitakul, A. Benyamin-Seeyar, and B. Eidson, "Frequency domain equalization for single-carrier broadband wireless systems," *IEEE Communications Magazine*, vol. 40, no. 4, pp. 58–66, 2002.

[4] H. Sari, G. Karam, and I. Jeanclaude, "Transmission techniques for digital terrestrial TV broadcasting," *IEEE Communications Magazine*, vol. 33, no. 2, pp. 100–109, 1995.

[5] A. Czylwik, "Comparison between adaptive OFDM and single carrier modulation with frequency domain equalization," in *Proceedings of IEEE 47th Vehicular Technology Conference (VTC '97)*, vol. 2, pp. 865–869, Phoenix, Ariz, USA, May 1997.

[6] A. Gusmão, R. Dinis, and N. Esteves, "On frequency-domain equalization and diversity combining for broadband wireless communications," *IEEE Transactions on Communications*, vol. 51, no. 7, pp. 1029–1033, 2003.

[7] D. D. Falconer and S. L. Ariyavisitakul, "Broadband wireless using single carrier and frequency domain equalization," in *Proceedings of the 5th International Symposium on Wireless Personal Multimedia Communications (WPMC '02)*, vol. 1, pp. 27–36, Honolulu, Hawaii, USA, October 2002.

[8] L. Martoyo, T. Weiss, F. Capar, and F. K. Jondral, "Low complexity CDMA downlink receiver based on frequency domain equalization," in *Proceedings of IEEE 58th Vehicular Technology Conference (VTC '03)*, vol. 2, pp. 987–991, Orlando, Fla, USA, October 2003.

[9] P. Schniter and H. Liu, "Iterative frequency-domain equalization for single-carrier systems in doubly-dispersive channels," in *Proceedings of the 38th Asilomar Conference on Signals, Systems, and Computers*, vol. 1, pp. 667–671, Pacific Grove, Calif, USA, November 2004.

[10] J. Alhava and M. Renfors, "Adaptive sine-modulated/cosine-modulated filter bank equalizer for transmultiplexers," in *Proceedings of the European Conference on Circuit Theory and Design (ECCTD '01)*, pp. 337–340, Espoo, Finland, August 2001.

[11] J. Alhava, A. Viholainen, and M. Renfors, "Efficient implementation of complex exponentially-modulated filter banks," in *Proceedings of IEEE International Symposium on Circuits and Systems*, vol. 4, pp. 157–160, Bangkok, Thailand, May 2003.

[12] A. Viholainen, J. Alhava, and M. Renfors, "Efficient implementation of complex modulated filter banks using cosine and sine modulated filter banks," *EURASIP Journal on Applied Signal Processing*, vol. 2006, Article ID 58 564, 10 pages, 2006.

[13] A. Viholainen, J. Alhava, and M. Renfors, "Efficient implementation of 2x oversampled exponentially modulated filter banks," *IEEE Transactions on Circuits and Systems II*, vol. 53, pp. 1138–1142, 2006.

[14] J. G. Proakis, *Digital Communications*, McGraw-Hill, New York, NY, USA, 4th edition, 2001.

[15] T. Ihalainen, T. Hidalgo Stitz, M. Rinne, and M. Renfors, "Channel equalization in filter bank based multicarrier modulation for wireless communications," to appear in EURASIP Journal of Applied Signal Processing.

[16] Y. Yang, T. Ihalainen, and M. Renfors, "Filter bank based frequency domain equalizer in single carrier modulation," in *Proceedings of the 14th IST Mobile and Wireless Communications Summit*, Dresden, Germany, June 2005.

[17] N. Benvenuto and S. Tomasin, "On the comparison between OFDM and single carrier modulation with a DFE using a frequency-domain feedforward filter," *IEEE Transactions on Communications*, vol. 50, no. 6, pp. 947–955, 2002.

[18] J. R. Treichler, I. Fijalkow, and C. R. Johnson Jr., "Fractionally spaced equalizers: how long should they really be?" *IEEE Signal Processing Magazine*, vol. 13, no. 3, pp. 65–81, 1996.

[19] P. Duhamel, "Implementation of split-radix FFT algorithms for complex, real, and real-symmetric data," *IEEE Transactions on Acoustics, Speech, and Signal Processing*, vol. 34, no. 2, pp. 285–295, 1986.

[20] H. S. Malvar, *Signal Processing with Lapped Transforms*, Artech House, Norwood, Mass, USA, 1992.

[21] A. Viholainen, T. Hidalgo Stitz, J. Alhava, T. Ihalainen, and M. Renfors, "Complex modulated critically sampled filter banks based on cosine and sine modulation," in *Proceedings of IEEE International Symposium on Circuits and Systems*, vol. 1, pp. 833–836, Scottsdale, Ariz, USA, May 2002.

[22] M. R. Petraglia, R. G. Alves, and P. S. R. Diniz, "New structures for adaptive filtering in subbands with critical sampling," *IEEE Transactions on Signal Processing*, vol. 48, no. 12, pp. 3316–3327, 2000.

[23] A. Viholainen, T. Ihalainen, T. Hidalgo Stitz, Y. Yang, and M. Renfors, "Flexible filter bank dimensioning for multicarrier modulation and frequency domain equalization,"

in *Proceedings of IEEE Asia Pacific Conference on Circuits and Systems*, pp. 451–454, Singapore, December 2006.

[24] T. Karp and N. J. Fliege, "Modified DFT filter banks with perfect reconstruction," *IEEE Transactions on Circuits and Systems II*, vol. 46, no. 11, pp. 1404–1414, 1999.

[25] T. Hentschel and G. Fettweis, *Software Radio Receivers*, Kluwer Academic, Boston, Mass, USA, 1999.

[26] S. Kay, *Fundamentals of Statistical Signal Processing: Estimation Theory*, Prentice-Hall, Englewood Cliffs, NJ, USA, 1993.

[27] W. W. Peterson and E. J. Weldon Jr., *Error-Correcting Codes*, MIT Press, Cambridge, Mass, USA, 2nd edition, 1972.

[28] T. B. Sorensen, P. E. Mogensen, and F. Frederiksen, "Extension of the ITU channel models for wideband OFDM systems," in *Proceedings of IEEE 62nd Vehicular Technology Conference (VTC '05)*, vol. 1, pp. 392–396, Dallas, Tex, USA, September 2005.

[29] R. G. Gallager, *Low-Density Parity-Check Codes*, MIT Press, Cambridge, Mass, USA, 1963.

[30] S. Hara, T. Matsuda, K. Ishikura, and N. Morinaga, "Co-existence problem of TDMA and DS-CDMA systems-application of complex multirate filter bank," in *Proceedings of IEEE Global Telecommunications Conference (GLOBECOM '96)*, vol. 2, pp. 1281–1285, London, UK, November 1996.

[31] M. J. Medley, G. J. Saulnier, and P. K. Das, "Narrow-band interference excision in spread spectrum systems using lapped transforms," *IEEE Transactions on Communications*, vol. 45, no. 11, pp. 1444–1455, 1997.

[32] T. Hidalgo Stitz and M. Renfors, "Filter-bank-based narrowband interference detection and suppression in spread spectrum systems," *EURASIP Journal on Applied Signal Processing*, vol. 2004, no. 8, pp. 1163–1176, 2004.

[33] Y. Yang, T. Hidalgo Stitz, M. Rinne, and M. Renfors, "Mitigation of narrowband interference in single carrier transmission with filter bank equalization," in *Proceedings of IEEE Asia Pacific Conference on Circuits and Systems*, pp. 749–752, Singapore, December 2006.

**Yuan Yang** received his B.S. degree in electrical engineering from HoHai University, Nanjing, China, in 1996, and his M.S. degree in information technology from Tampere University of Technology (TUT), Tampere, Finland, in 2001, respectively. Currently, he is a researcher and a postgraduate student at the Institute of Communications Engineering at TUT, working towards the doctoral degree. His research interests are in the field of broadband wireless communications, with emphasis in the topics of frequency-domain equalizers and multirate filter banks applications.

**Tero Ihalainen** received his M.S. degree in electrical engineering from Tampere University of Technology (TUT), Finland, in 2005. Currently, he is a researcher and a postgraduate student at the Institute of Communications Engineering at TUT, pursuing towards the doctoral degree. His main research interests are digital signal processing algorithms for multicarrier and frequency domain equalized single-carrier modulation based wireless communications, especially applications of multirate filter banks.

**Mika Rinne** received his M.S. degree from Tampere University of Technology (TUT) in signal processing and computer science, in 1989. He acts as Principal Scientist in the Radio Technologies laboratory of Nokia Research Center. His background is in research of multiple-access methods, radio resource management and implementation of packet decoders for radio communication systems. Currently, his interests are in research of protocols and algorithms for wireless communications including WCDMA, long-term evolution of 3G and beyond 3G systems.

**Markku Renfors** was born in Suoniemi, Finland, on January 21, 1953. He received the Diploma Engineer, Licentiate of Technology, and Doctor of Technology degrees from the Tampere University of Technology (TUT), Tampere, Finland, in 1978, 1981, and 1982, respectively. From 1976 to 1988, he held various research and teaching positions at TUT. From 1988 to 1991, he was a Design Manager at the Nokia Research Center and Nokia Consumer Electronics, Tampere, Finland, where he focused on video signal processing. Since 1992, he has been a Professor and Head of the Institute of Communications Engineering at TUT. His main research areas are multicarrier systems and signal processing algorithms for flexible radio receivers and transmitters.